

# Requirement of Mammalian *Timeless* for Circadian Rhythmicity

Jessica W. Barnes,<sup>1\*</sup> Shelley A. Tischkau,<sup>1,2\*</sup> Jeffrey A. Barnes,<sup>1\*</sup> Jennifer W. Mitchell,<sup>1</sup> Penny W. Burgoon,<sup>1</sup> Jason R. Hickok,<sup>1</sup> Martha U. Gillette<sup>1†</sup>

Despite a central circadian role in *Drosophila* for the transcriptional regulator *Timeless* (*dTim*), the relevance of mammalian *Timeless* (*mTim*) remains equivocal. Conditional knockdown of *mTim* protein expression in the rat suprachiasmatic nucleus (SCN) disrupted SCN neuronal activity rhythms, and altered levels of known core clock elements. Full-length *mTim* protein (mTIM-fl) exhibited a 24-hour oscillation, whereas a truncated isoform (mTIM-s) was constitutively expressed. mTIM-fl associated with the mammalian clock *Period* proteins (mPERs) in oscillating SCN cells. These data suggest that *mTim* is required for rhythmicity and is a functional homolog of *dTim* on the negative-feedback arm of the mammalian molecular clockwork.

An autoregulatory feedback loop of transcription and translation underlies generation of circadian rhythmicity in organisms ranging from cyanobacteria to mammals. Transcriptional activators, or positive elements, stimulate production of specific gene products that, in turn, act as transcriptional repressors, or negative elements, to feed back and inhibit their own transcription. The coordinated actions of positive and negative elements result in circadian expression patterns of clock and clock-controlled genes that drive oscillations in metabolism and behavior (1). An exception to homology between the *Drosophila* (2) and mammalian (3) clockworks is the *timeless* gene (*Tim*). The *dTim* gene is a critical

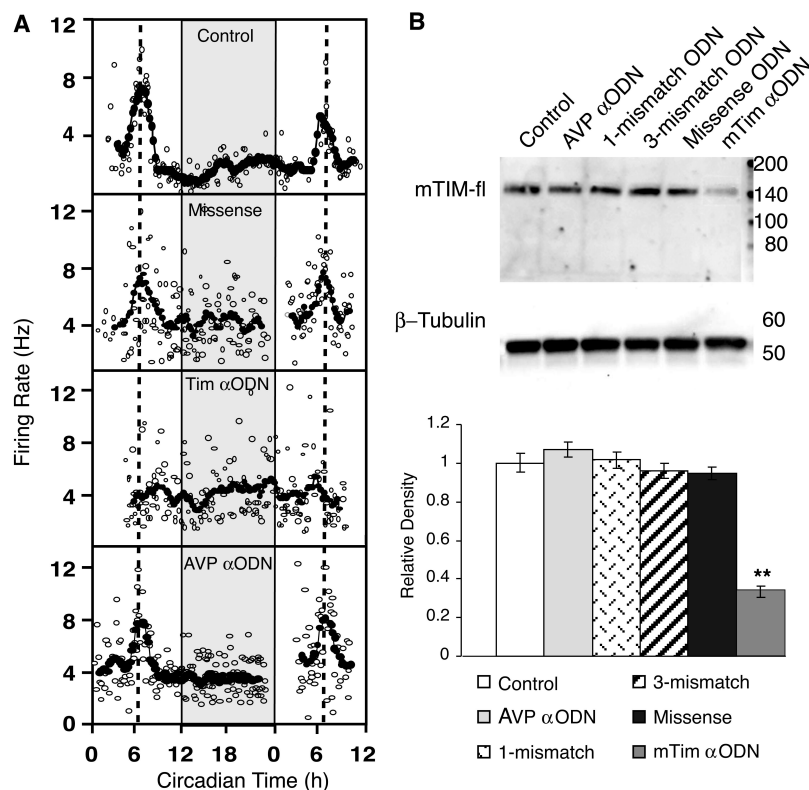
component in the autoregulatory feedback loop as homozygous *dTim* mutant flies are arrhythmic (4). In contrast, a clock function for *mTim* is ambiguous (5–14), and a requirement of *mTim* for circadian rhythmicity has not been firmly established. Attempts to address this question by genetic deletion of *mTim* have failed because the deletion of *mTim* is embryonically lethal [(6), supporting online material (SOM) text, note 1]. At present, a role for *mTim* in the mammalian circadian clock is largely discounted (15). To assess the requirement of *mTim* for circadian rhythmicity in the SCN, the site of the master circadian clock in mammals, we induced conditional knockdown of the full-length isoform of mTim protein (mTIM-fl) by treating SCN brain slices with antisense oligodeoxynucleotides ( $\alpha$ ODN) directed against the sequence surrounding the start codon of *mTim* (*mTim*  $\alpha$ ODN). This approach blocked mTIM-fl protein expression in kidney explant cultures (16), inhibited glutamate-induced phase shifts by targeting *mPer1* RNA (17–19), and disrupted VIP (vasoactive intestinal peptide) protein expression in the SCN (20, 21). SCN brain slices from rat maintained a circadian rhythm in neuronal firing rate with a peak near circadian time (CT) 7 over two cycles (22). Continuous exposure of SCN brain slices to *mTim*  $\alpha$ ODN significantly reduced mTIM-fl protein (Fig. 1B,  $P < 0.01$ , ANOVA, Tukey's *post hoc* analysis) and abolished the endogenous rhythm in neuronal firing rate compared with missense

<sup>1</sup>Department of Cell and Structural Biology, University of Illinois at Urbana-Champaign, Urbana, IL 61801, USA. <sup>2</sup>Department of Veterinary Biosciences, University of Illinois at Urbana-Champaign, Urbana, IL 61802, USA.

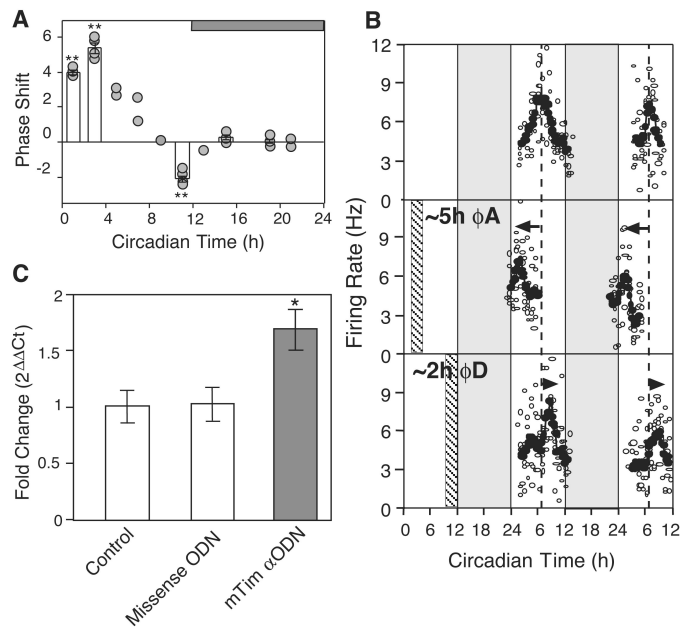
\*These authors contributed equally to this study.

†To whom correspondence should be addressed. E-mail: mgillett@uiuc.edu

**Fig. 1.** mTIM-fl knockdown abolishes SCN neuronal activity rhythms. (A) In control slices, the SCN maintained a circadian rhythm in neuronal firing rate with a peak near circadian time (CT) 7. Missense *mTim* ODN containing a scrambled sequence with no homology to other genes (as assessed by a GenBank BLAST search) had no effect on the rhythm of SCN neuronal firing rate. *mTim*  $\alpha$ ODN abolished the rhythm in neuronal firing rate. Firing-rate rhythms were normal after continuous treatment with  $\alpha$ ODN directed against arginine vasopressin (AVP  $\alpha$ ODN). Recordings shown are representative of 12 (control), 4 (missense), 3 (AVP  $\alpha$ ODN), or 6 (*mTim*  $\alpha$ ODN) independent experiments. Filled circles define the 2-hour running averages; open circles represent individual neuronal activities. Dashed line marks the mean time-of-peak in control SCN. Shading represents subjective night. ODN was applied from CT 2 on day 1 in vitro to CT 14 on day 2. (B) *mTim*  $\alpha$ ODN treatment significantly reduced mTIM-fl protein in SCN slices compared with no treatment, AVP  $\alpha$ ODN, one-mismatch, three-mismatch, and missense *mTim* ODN. SCN slices were collected after 36-hour treatment with ODN (22). Blots shown are representative of five independent experiments of *mTim*  $\alpha$ ODN, four independent experiments of missense *mTim* ODN and no treatment, three independent experiments using AVP  $\alpha$ ODN, one mismatch, and three mismatches. *mTim*  $\alpha$ ODN decreased mTIM-fl significantly. Molecular mass markers appear in the right lane. Density of mTIM-fl band was divided by the density of tubulin of the same lane. The mTIM-fl/tubulin ratio was normalized to control and plotted as the mean  $\pm$  SD. Double asterisks (\*\*) indicate statistical significance as determined by ANOVA ( $P < 0.01$ ) with Tukey's *post hoc* analysis.



REPORTS



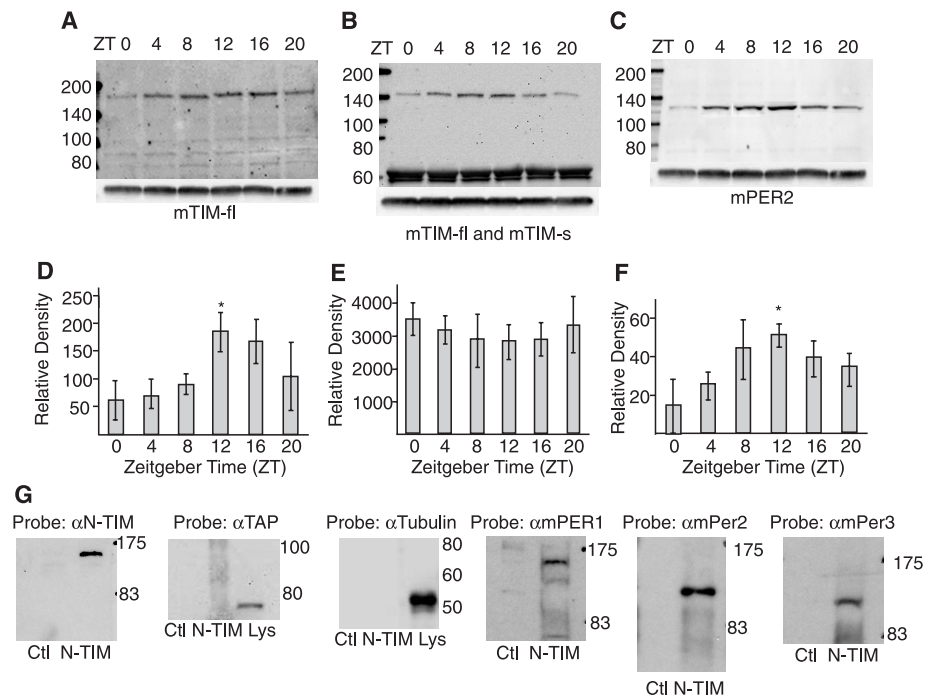
indicated by filled circles. **(B)** Control slices displayed a characteristic rhythm in the firing rate of the SCN neuronal ensemble with a peak near CT 7. *mTim*  $\alpha$ ODN induced maximal phase advance when applied from CT 2 to CT 4. *mTim*  $\alpha$ ODN caused phase delay when applied from CT 10 to CT 12. Slash-filled bars represent time and duration of short-term *mTim*  $\alpha$ ODN treatment. The labels ~5h  $\phi$ A and ~2h  $\phi$ D denote a phase advance of about 5 hours and a phase delay of about 2 hours, respectively. **(C)** After treatment of SCN slices with *mTim*  $\alpha$ ODN, or missense *mTim* ODN from CT3 to CT5, *mTim-fl* transcript level in single SCN slices was determined by qPCR. Because *mTim-fl* level in missense-treated slices ( $n = 4$ ) was not different from untreated samples ( $n = 3$ ), these samples were pooled for statistical analysis. *mTim-fl* was increased significantly ( $1.68 \pm 0.18$ -fold,  $P < 0.05$ , Student's  $t$  test,  $n = 4$ ) after *mTim*  $\alpha$ ODN treatment compared with missense and untreated controls. Asterisk (\*) indicates statistical significance as determined by Student's  $t$  test ( $P < 0.05$ ).  $2^{\Delta\Delta Ct}$  gives the fold change in gene expression between the two groups (22).

**Fig. 2.** Short-term treatment with *mTim*  $\alpha$ ODN causes phase resetting in the SCN and increases *mTim-fl* transcript levels. **(A)** A phase-response curve was derived from 25 experiments over 10 different time points across the circadian cycle to assess sensitivity to 2-hour treatment with *mTim*  $\alpha$ ODN. Phase advances in response to treatment were observed during early subjective day, phase delays during late subjective day, and no change in the SCN neuronal activity rhythm during subjective night (dark horizontal bar). Double asterisks indicate statistical significance as determined by Student's  $t$  test ( $P < 0.01$ ). Independent experiments are

and antisense ODN that targeted arginine vasopressin (*AVP*  $\alpha$ ODN) controls (Fig. 1A; SOM text, note 2). The *mTim*  $\alpha$ ODN effect was specific: long-term exposure of SCN brain slices to *mTim*  $\alpha$ ODN containing one or three mismatched bases had no effect on mTIM-fl protein levels (Fig. 1B) or the SCN rhythm of neuronal firing (SOM text, note 3).

To determine whether *mTim* acts as a state variable, the neuronal firing-rate rhythm of SCN slices was determined in response to transient inhibition of *mTim-fl* expression (17–19). Short treatments (2 hours) with *mTim*  $\alpha$ ODN caused significant phase shifts in SCN firing-rate rhythms when applied during subjective day but had no effect when applied during subjective night (Fig. 2A). Control slices displayed a characteristic rhythm in the firing rate of the SCN neuronal ensemble (mean time of peak = CT  $6.72 \pm 0.12$ ,  $n = 12$ , Fig. 2B). *mTim*  $\alpha$ ODN induced phase advances when applied between CT 0 and CT 8; maximal advances of ~5.5 hours ( $P < 0.01$ , Student's  $t$  test) in the time-of-peak activity were observed with *mTim*  $\alpha$ ODN treatment from CT 2 to CT 4 (mean time of peak CT  $1.15 \pm 0.25$ ,  $n = 4$ , Fig. 2, A and B). *mTim*  $\alpha$ ODN caused phase delays ( $P < 0.05$ , Student's  $t$  test) when applied during late subjective day (CT 10 to CT 12; mean time of peak CT  $8.82 \pm 0.13$ ,  $n = 4$ , Fig. 2, A and B). Treatment with missense *mTim* ODN had no effect on SCN rhythmicity at any time of day. Thus, phasing of SCN rhythmicity was altered when transcriptional

**Fig. 3.** Rhythmic expression of mTIM-fl, but not mTIM-s, in the SCN and mTIM-fl:mPER interactions in the SCN 2.2 cell line. Protein extracts from SCN collected at 4-hour intervals were analyzed by Western blot immunoreactivity (22) and were quantified for the N-terminal (A and D), C-terminal (B and E), and mPER2 (C and F) antisera. Duplicate blots were prepared and probed with the N or C terminal-specific antiserum (22). Blots probed with N-terminal antiserum were stripped and reprobed for mPER2. Blots were subsequently stripped and reprobed for  $\beta$ -tubulin (A, B, and C, bottom row). Distinct rhythmic expression in the SCN was seen in mTIM-fl and mPER2, but not mTIM-s over a full 24-hour cycle (D, E, and F); Asterisk indicates  $P < 0.05$ , Student's  $t$  test of ZT 0 versus ZT 12. Blots shown are representative of independent experiments and analysis (mTIM-fl and mTIM-s over the full circadian cycle,  $n = 4$ ). **(G)** N terminal-specific mTIM antiserum immunoprecipitated mTIM-fl from SCN 2.2 cell lysate. mPER1, mPER2, and mPER3 coimmunoprecipitated with mTIM-fl in the SCN 2.2 cell line, whereas  $\beta$ -tubulin and TAP (SOM text, note 10) did not. Lanes on each blot are labeled with cell lysate or the antiserum (CTL, rabbit control IgG; N-TIM, N terminal-specific mTIM antiserum) used for immunoprecipitation. The antiserum used to probe each respective membrane is labeled above the blot. Results are representative of at least three separate experiments. Molecular mass markers are present on the interface of the blots in the left lanes of (A, B, and C); and in the right lanes of (G).



and translational events involving mRNA encoding *mTim-fl* were transiently disrupted.

To evaluate the means by which transient exposure to *mTim*  $\alpha$ ODN alters circadian timing, we analyzed the level *mTim-fl* mRNA by quantitative real-time reverse transcription polymerase chain reaction (qPCR). Treatment with *mTim*  $\alpha$ ODN from CT 3 to CT 5 caused a significant increase ( $1.68 \pm 0.14$  fold,  $n = 4$ ,  $P < 0.05$ , Student's *t* test) in *mTim-fl* transcript levels (Fig. 2C). Levels of *mTim-fl* mRNA in slices treated with missense *mTim* ODN were not different from untreated slices. Because this *mTim*  $\alpha$ ODN treatment predicts clock resetting to the end of subjective day, when clock-controlled *mTim-fl* mRNA levels rise (13), the consequence of *mTim*  $\alpha$ ODN on *mTim-fl* mRNA was consistent with the effect on phasing of the SCN neuronal activity rhythm. This effect of altering *mTim* transcription and translation suggests that *mTim* is a critical state variable, and its disruption alters circadian timing.

Two transcripts of *mTim* RNA are present in other mammalian tissues and show differential expression in the tissues of developing and adult mouse (16). The larger transcript, which is less abundant in adult tissues, encodes mTIM-fl (SOM text, note 4). The shorter transcript, which is a splice variant of the full-length transcript and encodes a protein that corresponds to the last 475 residues of the mTIM-fl protein, has been designated TIMELESS small isoform [mTIM-s (16)]. To examine the expression of each of these mTIM isoforms in the SCN and their potential contributions to the circadian clockwork, we generated antisera against the N- and C-terminal regions of mTIM (fig. S1A). Analysis of SCN extracts using N terminal-specific antiserum identified a single immunoreactive

protein of  $\sim 140$  kD (fig. S1B), corresponding to mTIM-fl (SOM text, note 5). Immunoreactivity disappeared after treatment of SCN slices with *mTim*  $\alpha$ ODN or after absorption of the antibody with the corresponding peptide. In contrast, analysis of SCN extracts with C terminal-specific mTIM antiserum revealed immunoreactive proteins at  $\sim 140$  kD and  $\sim 50$  kD; immunoreactivity was abolished by absorption of antiserum with the corresponding peptide (fig. S1C). The  $\sim 50$ -kD protein band resolved as a triplet with the C terminal-specific antiserum and corresponds to the predicted size of mTIM-s.

mTIM-fl detected by the N terminal-specific antiserum exhibited a significant ( $P < 0.05$ , Student's *t* test) and robust oscillation (3.8-fold) in the SCN (Fig. 3, A and D) with peak levels occurring at zeitgeber time 12 (ZT 12), the time of lights off. SCN extracts blotted with the C terminal-specific antiserum also showed a significant oscillation in mTIM-fl ( $P < 0.01$ , Student's *t* test) but no significant variation in the more abundant mTIM-s (Fig. 3, B and E; SOM text, note 6). An oscillation of the *Period* protein mPER2 (3.75-fold) that peaked between ZT 8 and ZT 12, similar to that reported in mouse (5) and parallel to mTIM-fl, was present in the same samples (Fig. 3, C and F; SOM text, note 7). The more abundant alternative splice variant that encodes the truncated mTIM-s protein provides an explanation for a previous report of constitutive expression of mTIM-fl in immunostained tissue [(5, 23), SOM text, note 8].

If mTIM-fl is a core clock component, it should interact with other clock elements. Interactions between mTIM-fl and the mammalian clock *Cryptochrome* proteins (mCRYs) have been reported in vitro and in vivo (5, 7, 9). To examine whether mTIM-fl

interacts with other negative regulators of the mammalian clockwork in vivo, we probed a rat SCN-derived cell line [SCN 2.2 (24)] for interactions between mTIM-fl and the three mammalian clock *Period* proteins (mPERs). N terminal-specific antiserum immunoprecipitated mTIM-fl and coimmunoprecipitated mPER1, mPER2, and mPER3 from SCN 2.2 cell extracts [Fig. 3G, (22); SOM text, note 9]. Association of mTIM-fl with mPERs and mCRYs in vivo (5, 7, 9), as well as studies that show mTIM-fl inhibits mCLK:BMAL- and MOP4:BMAL-induced *mPER1* gene transactivation in vitro in a dose-dependent manner (7, 9, 11), further support mTIM-fl as a core clock element.

If mTIM-fl plays an important role in the mammalian clockwork, its knockdown should disrupt expression levels of other key elements in the feedback loop. *mTim*  $\alpha$ ODN treatment caused a significant decrease ( $P < 0.001$ , Student's *t* test) in the levels of mPER1, mPER2, and mPER3 (Fig. 4, A to C) and a significant increase ( $P < 0.001$ , Student's *t* test) in the levels of mCRY1 and mCRY2 (Fig. 4, D and E) compared with missense ODN-treated or control SCN brain slices. Experiments using double-stranded RNA interference in HEK 293 cells produced similar decreases in hPER2 levels (fig. S3) and overexpression of mTIM-fl in HEK 293 cells resulted in increased levels of hPER2 (fig. S4). In *Drosophila*, *timeless* mutant flies have constitutively low levels of PERIOD (25). Given that dTIM has been shown to contribute importantly to the expression and stability of dPER, the effect of mTIM-fl knockdown on the mPERs indicates that mTIM-fl is a functional homolog of dTIM.

The data presented here provide functional evidence that mTIM-fl is required for expression of SCN circadian rhythmicity. These findings permit us to reconfigure the current model of the mammalian circadian clockwork. The aggregate evidence places *mTim* on the negative arm of the molecular feedback loop in the SCN, as it is in the *Drosophila* clock. We hypothesize that mPER2 may be the physiologically preferred partner of mTIM-fl and that this heterodimer could be the functional mammalian counterpart of dTIM:dPER. Addition of *mTim* to the mammalian clockwork completes a core having each functional homolog of the *Drosophila* clockwork and emphasizes the highly conserved nature of the biological timekeeping mechanism.

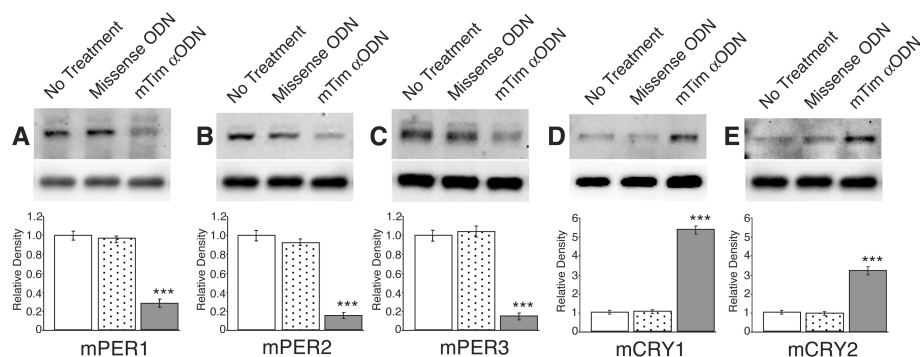


**Fig. 4.** mTIM-fl knockdown disrupts expression levels of other core clock elements. SCN brain slices treated identically to those in Fig. 1B were Western blotted (22) for other components of the mammalian molecular clockwork. mTIM-fl knockdown caused a significant reduction of mPER1 (A), mPER2 (B), and mPER3 (C) levels. mTIM-fl knockdown caused a significant increase in mCRY1 (D) and mCRY2 (E).  $P < 0.001$ , Student's *t* test for both *mTim*  $\alpha$ ODN versus missense ODN and *mTim*  $\alpha$ ODN versus control samples,  $n = 4$  for each treatment). Density of the clock protein band (top row of blot) was divided by the density of tubulin (middle row) of the same lane. The clock protein/tubulin ratio was normalized to control and plotted as the mean  $\pm$  SD (bottom row). Triple asterisks indicate statistical significance as determined by Student's *t* test ( $P < 0.001$ ).

#### References and Notes

1. J. C. Dunlap, *Cell* **96**, 271 (1999).
2. M. W. Young, S. A. Kay, *Nature Rev. Genet.* **2**, 702 (2001).
3. D. P. King, J. S. Takahashi, *Annu. Rev. Neurosci.* **23**, 713 (2000).
4. A. Sehgal, J. L. Price, B. Man, M. W. Young, *Science* **263**, 1603 (1994).
5. M. D. Field et al., *Neuron* **25**, 437 (2000).

6. A. L. Gotter *et al.*, *Nature Neurosci.* **3**, 755 (2000).
7. E. A. Griffin Jr., D. Staknis, C. J. Weitz, *Science* **286**, 768 (1999).
8. N. Koike *et al.*, *FEBS Lett.* **441**, 427 (1998).
9. K. Kume *et al.*, *Cell* **98**, 193 (1999).
10. S. Sakamoto *et al.*, *Biochem. Biophys. Res. Commun.* **279**, 131 (2000).
11. A. M. Sangoram *et al.*, *Neuron* **21**, 1101 (1998).
12. T. Takumi *et al.*, *Genes Cells* **4**, 67 (1999).
13. S. A. Tischkau *et al.*, *J. Neurosci.* **19**, RC15 (1999).
14. M. J. Zylka *et al.*, *Neuron* **21**, 1115 (1998).
15. U. Albrecht, *J. Appl. Physiol.* **92**, 1348 (2002).
16. Z. Li *et al.*, *Proc. Natl. Acad. Sci. U.S.A.* **97**, 10038 (2000).
17. M. Akiyama *et al.*, *J. Neurosci.* **19**, 1115 (1999).
18. S. A. Tischkau, J. W. Mitchell, S. H. Tyan, G. F. Buchanan, M. U. Gillette, *J. Biol. Chem.* **278**, 718 (2003).
19. H. Wakamatsu *et al.*, *Neuroreport* **12**, 127 (2001).
20. L. M. Gerhold, M. T. Sellix, M. E. Freeman, *J. Comp. Neurol.* **450**, 135 (2002).
21. J. P. Harney, K. Scarbrough, K. L. Rosewell, P. M. Wise, *Endocrinology* **137**, 3696 (1996).
22. Materials and methods are available as supporting material on Science Online.
23. M. H. Hastings, M. D. Field, E. S. Maywood, D. R. Weaver, S. M. Reppert, *J. Neurosci.* **19**, RC11 (1999).
24. D. J. Earnest, F. Q. Liang, M. Ratcliff, V. M. Cassone, *Science* **283**, 693 (1999).
25. J. L. Price, M. E. Dembinska, M. W. Young, M. Rosbash, *EMBO J.* **14**, 4044 (1995).
26. The authors thank L. Levesque for her generous gift of TAP antiserum. Supported by Public Health Service Grants NS22155, NS35859, HL67007, and a University Scholar award (M.U.G.); GM07143 (J.W.B., J.A.B.); NS10170 (S.A.T.); NS11158

(J.W.M.); NS11134 (P.W.B.); and a grant from the Illinois Governor's Venture Technology Fund/Molecular & Endocrine Pharmacology Program (S.A.T.). Opinions, findings, and conclusions or recommendations expressed herein are those of the authors and do not necessarily reflect the views of funding agencies.

#### Supporting Online Material

www.sciencemag.org/cgi/content/full/302/5644/439/DC1

Materials and Methods

SOM Text

Figs. S1 to S4

References

8 May 2003; accepted 5 September 2003

## Diffusion Dynamics of Glycine Receptors Revealed by Single-Quantum Dot Tracking

Maxime Dahan,<sup>1\*</sup> Sabine Lévi,<sup>2\*</sup> Camilla Luccardini,<sup>1</sup> Philippe Rostaing,<sup>2</sup> Béatrice Riveau,<sup>2</sup> Antoine Triller<sup>2†</sup>

Semiconductor quantum dots (QDs) are nanometer-sized fluorescent probes suitable for advanced biological imaging. We used QDs to track individual glycine receptors (GlyRs) and analyze their lateral dynamics in the neuronal membrane of living cells for periods ranging from milliseconds to minutes. We characterized multiple diffusion domains in relation to the synaptic, perisynaptic, or extrasynaptic GlyR localization. The entry of GlyRs into the synapse by diffusion was observed and further confirmed by electron microscopy imaging of QD-tagged receptors.

In living cells, the ability to selectively detect one molecule (or a small number of molecules) is a powerful way to understand the dynamics of cellular organization (1). So far, access to single-molecule properties in living cells has been restricted by either the size of the probe (40-nm gold nanoparticles or 500-nm latex spheres) (2) or the photobleaching of the small (1- to 4-nm) fluorescent labels (3, 4). QDs, which are intermediary in size (~5 to 10 nm), are substantially more photostable than conventional fluorophores (5, 6), and have been vaunted as promising fluorescent probes (6, 7). In vitro and in vivo imaging with QDs has recently been demonstrated, but none of these measurements has aimed at specific cellular actors (8, 9).

GlyR is the main inhibitory neurotransmitter receptor in the adult spinal cord (10). At inhibitory synapses, GlyR clusters are stabilized

by the scaffolding protein gephyrin (11, 12). The issue of lateral mobility of receptors for neurotransmitters has become central to understanding the development and plasticity of synapses (13). The membrane dynamics of GlyRs has been studied previously in transfected neurons using latex beads (14). GlyRs diffuse rapidly in the neuronal plasma membrane and transient interaction with gephyrin decreases their diffusion. Comparable results were obtained for the metabotropic- and AMPA-type glutamate receptors and their corresponding scaffolding molecules (15, 16). These measurements, however, preclude analysis of receptor dynamics in the synaptic cleft because of the use of 500-nm beads. We aimed to develop a new approach that could both access the synapse and be tracked for long periods of time.

The specific detection of endogenous GlyR  $\alpha 1$  subunits at the surface of spinal cultured neurons was achieved by the use of a primary antibody (mAb2b), biotinylated anti-mouse Fab fragments, and streptavidin-coated QDs (Fig. 1) (17). QD-GlyR formed numerous clusters around the soma and dendrites (Fig. 1A), similar to observations from previous immunocytochemical studies using conventional fluorophores (18). GlyRs were detected within synaptic and extrasynaptic domains (Fig. 1, B and C).

QDs were then used to study the lateral movement of individual GlyRs in living neurons. Single QDs were identified by their blinking property, i.e., the random intermittency of their fluorescence emission (5, 19). The results of these experiments were compared with those that used Cy3-coupled antibodies. Trajectories of single QD-GlyRs in the membrane could be visualized easily for at least 20 min, whereas the duration was ~5 s for Cy3. The spots were detected with a signal-to-noise ratio of about 50 (integration time 75 ms), almost an order of magnitude higher than the signal obtained with fluorophores. Thus, the lateral resolution reached 5 to 10 nm, well below the 40 nm achieved with Cy3 dyes (20).

First, we used single-QD tracking (SDQT) to study the rapid lateral dynamics of GlyRs. Continuous sequences of 75-ms images were acquired for durations of ~60 s. Individual QD-GlyRs diffusing in the neuronal membrane were either detected in extrasynaptic regions or associated with boutons identified with the amphiphilic FM4-64 dye. SDQT enabled the observation of multiple exchanges between extrasynaptic and synaptic domains, in which a GlyR alternated between free and confined diffusion states, respectively (Fig. 2A and movie S1). A GlyR, initially located at a synapse, started to diffuse rapidly (Fig. 2, A1 to A5) and, after about 30 s, stabilized close to another synaptic site (Fig. 2, A6 to A8), 4 to 5  $\mu\text{m}$  away from the starting point. To quantify this observation, the instantaneous diffusion coefficients ( $D$ ) were determined along the trajectory (Fig. 2B). For the 0- to 30-s period,  $D$  was ~0.1  $\mu\text{m}^2/\text{s}$ , and the mean-square displacement (MSD) function varied linearly (Fig. 2C), as is expected for free Brownian diffusion (2). In the later part of the trajectory (30 to 63 s),  $D$  decreased to ~0.02  $\mu\text{m}^2/\text{s}$ , and the MSD exhibited a negative curvature, characteristic of a space-confined movement (Fig. 2D).

The high photostability of QDs also allowed for the tracking of individual GlyRs in the same neuritic region for long durations. To avoid toxic continuous illumination of the cells, data were acquired in a

<sup>1</sup>Laboratoire Kastler Brossel, CNRS UMR 8552, Ecole Normale Supérieure and Université Pierre et Marie Curie, 24 rue Lhomond, 75005 Paris, France. <sup>2</sup>Biologie Cellulaire de la Synapse, INSERM U497, Ecole Normale Supérieure, 46 rue d'Ulm, 75005 Paris, France.

\*These authors contributed equally to this work.  
†To whom correspondence should be addressed. E-mail: maxime.dahan@lkb.ens.fr (M.D.); triller@wotan.ens.fr (A.T.)